Sources and composition of fluids associated with fluorite deposits of Asturias (N Spain)

V. SÁNCHEZ [1], E. VINDEL [1], T. MARTÍN-CRESPO[2], M. CORBELLA[3], E. CARDELLACH[3] AND D. BANKS[4]

ABSTRACT

The fluorite deposits of Asturias (northern Iberian Peninsula) are hosted by rocks of Permo-Triassic and Palaeozoic age. Fluid inclusions in ore and gangue minerals show homogenization temperatures from 80 to 170°C and the presence of two types of fluids: an H_2O–NaCl low-salinity fluid (<8 eq. wt% NaCl) and an H_2O–NaCl–$CaCl_2$ fluid (7–13 wt% NaCl and 11–14 wt% $CaCl_2$). The low salinity and the Cl/Br and Na/Br ratios (Cl/Br_{molar} 100–700 and Na/Br_{molar} 20–700) are consistent with an evaporated sea water origin of this fluid. The other end-member of the mixture was highly saline brine with high Cl/Br and Na/Br ratios (Cl/Br_{molar} 700–13 000 and Na/Br_{molar} 700–11 000) generated after dissolution of Triassic age evaporites. LA-ICP-MS analyses of fluid inclusions in fluorite reveal higher Zn, Pb and Ba contents in the high-salinity fluids (160–500, 90–170, 320–480 p.p.m. respectively) than in the low-salinity fluid (75–230, 25–150 and 100–300 p.p.m. respectively). The metal content of the fluids appears to decrease from E to W, from Berbes to La Collada and to Villabona. The source of F is probably related to leaching of volcanic rocks of Permian age. Brines circulated along faults into the Palaeozoic basement. Evaporated sea water was present in permeable rocks and faults along or above the unconformity between the Permo-Triassic sediments and the Palaeozoic basement. Mineralization formed when the deep brines mixed with the surficial fluids in carbonates, breccias and fractures resulting in the formation of veins and stratabound bodies of fluorite, barite, calcite, dolomite and quartz and minor amounts of sulphides. Fluid movement and mineralization occurred between Late Triassic and Late Jurassic times, probably associated with rifting events related to the opening of the Atlantic Ocean. This model is also consistent with the geodynamic setting of other fluorite-rich districts in Europe.

Key words: crush-leach, fluid inclusions, fluorite, genetic model, LA-ICP-MS

INTRODUCTION

Brines are common mineralizing fluids in sedimentary-hosted ore deposits, but the source of their solutes as well as the metal content remains uncertain in many cases. Recent advancements in analytical techniques applied to fluid inclusions such as Laser ablation-inductively coupled plasma mass spectrometry combined with other geochemical data (microthermometry and crush-leach analyses) can help to characterize not only the metal contents of the fluids but also the source of their major and minor components.

The fluorspar district of Asturias (northern Iberian Peninsula) has been one of the major fluorite producers in Europe with approximately 40 known occurrences (García Iglesias & Loredo 1994) producing more than 15 Mt of ore since the 1970s. This economically important mineralization is found in three districts, Berbes, La Collada and Villabona, where three mines are currently in operation: Emilio in Berbes, La Viesca in La Collada and Moscona in Villabona (Fig. 1). Mineralization occurs as vein and stratabound bodies in highly silicified red-bed sediments (marls and sandstones), carbonates and calcareous breccias of Permo-Triassic age (García Iglesias & Loredo 1994), and

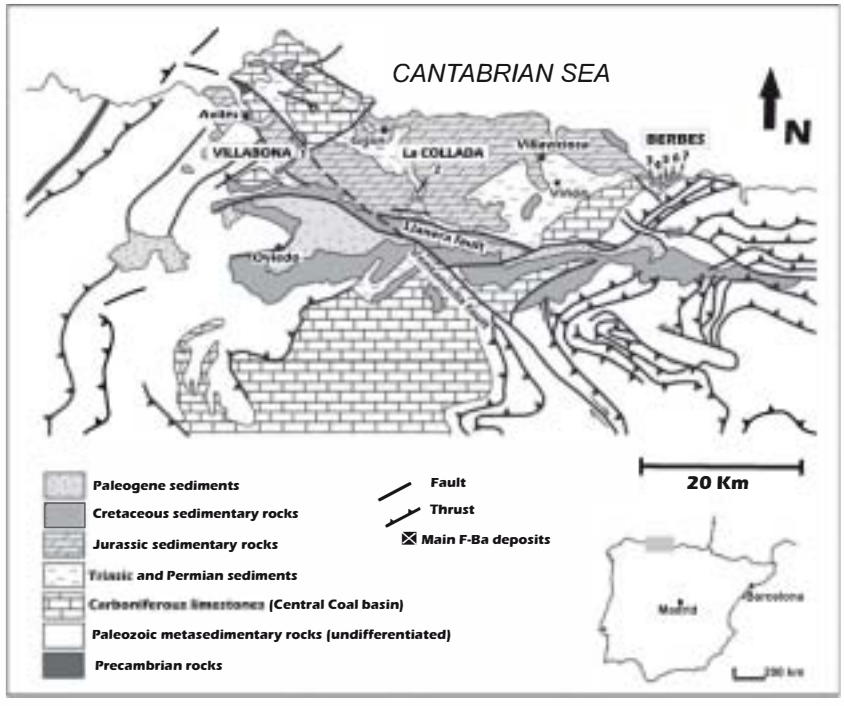

Fig. 1. Simplified geological map of the Asturias region showing the location of fluorite deposits and mining districts. (1) Moscona Mine, (2) La Viesca Mine, (3) Emilio Mine, (4) Valnegro, (5) Aurora vein, (6) San Lino Mine, (7) El Frondil ''La Paredona''.

as veins hosted in limestones of the Carboniferous basement.

The Asturian deposits are apparently similar to other fluorite and Ba–Zn–Pb mineralization in Europe, located near the contact between Variscan and Mesozoic rocks, e.g. the F–Ba veins in the Pyrenees (Johnson *et al.* 1996; Subias *et al.* 1998) and in the Catalonian Coastal Ranges (Canals *et al.* 1992; Canals & Cardellach 1993); the F veins in the Massif Central (Lhégu *et al.* 1982; Sizaret *et al.* 2004); and the Pb–Zn–F–Ba mineralization in SW Germany (von Gehlen 1989) and the North Pennine Orefield (Dunham 1990) and south-west England (Gleeson *et al.* 2001). F–Ba(–Zn–Pb) mineralization has been related to hydrothermal activity associated with extensional rift regimes developed during the opening of the N Atlantic, from Jurassic to Cretaceous times and share the geochemical characteristics of Mississippi Valley Type (MVT) deposits. Sánchez *et al.* (2006) obtained a Sm–Nd isochron on fluorite from Villabona that yielded an age of 185 ± 28 Myr, MSWD = 0.3 (Late Triassic–Late Jurassic).

Previous geological, geochemical and mineralogical studies of the Asturian fluorite deposits were performed by García Iglesias (1978), Ferrand *et al.* (1978), Garcia Iglesias & Loredo (1992), García Iglesias & Loredo (1994), García Iglesias & Touray (1977), Loredo & Garcia Iglesias (1984) and Tejerina & Zorrilla (1980). This study presents new insights into the composition of the mineralizing fluids of the fluorspar district of Asturias derived from two approaches: microthermometric and halogen data from fluid inclusions trapped in fluorite, quartz, calcite and barite; and quantitative analysis of the metal content in fluids using the LA-ICP-MS technique (Günther *et al.* 1997, 1998; Heinrich *et al.* 2003), in order to better understand the fluid sources and evolution, flow pathways and ore-forming conditions at a regional scale. Finally, a genetic model of the hydrothermal mineralization is outlined and compared with other known fluorite districts.

GEOLOGICAL SETTING

Two geological provinces can be distinguished in the Asturian region. The westernmost area is composed of Precambrian and Palaeozoic rocks (Fig. 1) comprising the folded and fractured Variscan basement. The Palaeozoic rocks consist of Cambrian limestones and sandstones as well as Ordovician and Devonian quartzites. The thickest sequence of sediments is of Carboniferous age, consisting of alternating carbonate and siliciclastic units (Aller 1986). The basement represents a Variscan, east-vergent, arcuate, thin-skinned foreland thrust and fold belt (Julivert 1971; Pérez-Estaún *et al.* 1988) which was uplifted during the Alpine orogeny over two synorogenic Tertiary basins: the Duero basin in the south and the Bay of Biscay in the north (Alonso & Pulgar 1995).

The central and easternmost areas of the region comprise Mesozoic and Cenozoic units that unconformably overlie the Palaeozoic basement (Fig. 1). Here, the oldest rocks are Permo-Triassic red mudstones, evaporites and calcarenites, interbedded with thin (<30 m) lava and pyroclastic flows in the Villaviciosa area. These volcanic rocks

are basaltic to andesitic–trachytic in composition (53–61 wt% SiO_2) and belong to the high-K, calc-alkaline series (Valverde 1993). In these rocks, an intense hydrothermal alteration (seritization) has been identified by the presence of numerous pseudomorphs after plagioclase, olivine and pyroxene crystals in an aphanitic matrix. According to García Iglesias & Loredo (1994), these volcanic rocks are regionally enriched in fluorine.

During the Jurassic, the Asturian basin was part of a large epicontinental sea, bounded by the Iberian Massif to the south-west and by the Armorican Massif to the north. Tectonic activity at the Triassic–Jurassic transition was related to extensional movements leading to the westward extension of the Tethys Ocean. More extensional tectonics took place during the Late Jurassic–Early Cretaceous, linked to the opening of the central Atlantic and the Bay of Biscay (Salas *et al.* 2001), which produced the most important Mesozoic basins of Europe. The fluorite deposits analysed in this study were emplaced in structures related to the Late Jurassic–Early Cretaceous extension event.

The area studied is located in central and eastern Asturias within the Mesozoic basin. The Berbes district is located in its easternmost zone (Fig. 1) and contains Emilio, the only mine currently in operation, as well as several abandoned deposits (El Frondil or La Paredona, San Lino, Aurora and Valnegro). Mineralization occurs as veins hosted in Carboniferous limestones (Aurora Mine) and as stratabound bodies hosted in breccio-conglomerates of Permo-Triassic age that unconformably overlie the Carboniferous limestones (Sánchez de la Torre *et al.* 1977; Tejerina & Zorrilla 1980; Fernández 1995). The breccias are composed of carbonate fragments of Carboniferous carbonate and are cemented by a grey to brownish carbonated matrix. These breccias are related to a Palaeozoic palaeo-relief and their largest outcrop extent is found in areas close to fractures affecting the basement. Fluorite fills centimetre to metre-thick veins and dissolution cavities and replaces some of the clasts. Mineralization terminates abruptly where the breccia changes to Triassic marls and sandstones (García Iglesias & Loredo 1994).

The geology and the stratigraphic section in La Collada (Fig. 1) are similar to those in Berbes and were described in detail by Martínez-García & Tejerina (1979). Fluorite is present again in veins and stratabound bodies hosted in Permo-Triassic rocks that unconformably overlie the Palaeozoic basement. Mineralization is controlled by fractures that follow two major structures, the NW–SE-trending Ventaniella Fault, which constitutes the south-western limit of the Jurassic basin, and the E–W-trending Llanera Fault. Veins outnumber breccia replacements, which decrease towards the Upper Triassic marls in the upper parts of the formation. Samples for this study were collected from the currently active mine of La Viesca.

The Villabona district, located 10 km south of the town of Avilés (Fig. 1) includes the most important active mine in the region, Moscona Mine. The district is located at the intersection of the Ventaniella Fault with the Llanera Fault. The mineralization consists of replacement (stratabound) and vein bodies. Unlike in Berbes and La Collada, the lower breccio-conglomerated unit is removed in Villabona.

MINERALOGY AND PARAGENETIC SEQUENCE

The mineralogy of the deposits in the three districts studied is very similar and comprises fluorite, barite, calcite, dolomite, quartz and minor amounts of sulphides: pyrite, galena, chalcopyrite and marcasite. The paragenetic succession is shown in Fig. 2.

Mineralization was preceded by a widespread silicification (microcrystalline quartz Q1) (Fig. 3A) dolomitization and chloritization of the host rocks. Fluorite precipitation took place either as replacement or in open space fillings.

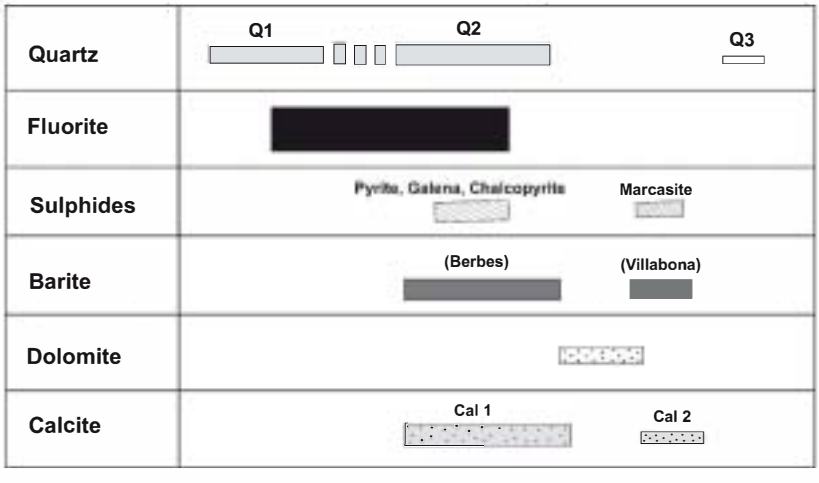

Fig. 2. Paragenetic sequence in the Asturias deposits.

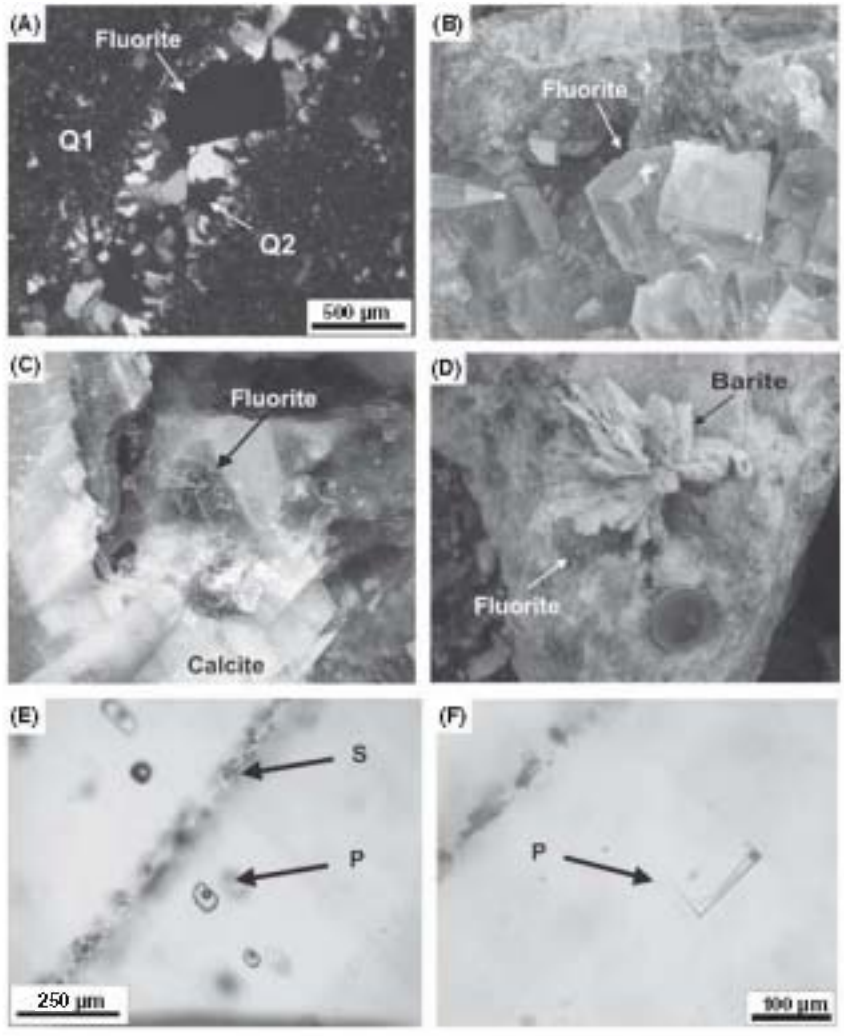

Fig. 3. (A) Fluorite and drusy clear quartz crystals (Q2) filling a vein cutting an aggregate of microcrystalline quartz (Q1). (B) Colourless, cubic fluorite crystals, 'La Viesca' mine, La Collada district. (C) Calcite rhombohedrons surrounding purple fluorite, 'La Viesca' mine, La Collada district. (D) Barite in rosettes or platy aggregates associated with purple fluorite, 'La Paredona' area, Berbes district. (E) Primary fluid inclusions (P) in fluorite, distributed along growth planes parallel to crystal faces, and secondary fluid inclusions (S) scattered along a healed fracture. (F) Primary (P) fluid inclusion isolated in fluorite crystal.

In the Berbes and La Collada districts, fluorite occurs as cubic, uncoloured, deep purple, green or blue crystals (Fig. 3B); in the Villabona district, fluorite is predominantly yellow, with a purple colour appearing occasionally at the edge of some yellow crystals. Sulphides precipitated during and after fluorite formation, as shown by the presence of pyrite and chalcopyrite crystals either enclosed by or growing over fluorite. A second generation of drusy quartz (Q2) precipitated simultaneously and after fluorite, and was followed by both calcite, a pervasive mineral in the three districts, and dolomite. Two generations of calcite (cal 1 and cal 2) have been recognized: (i) early idiomorphic crystals that grow over fluorite (Fig. 3C) and (ii) late calcite scalenohedrons mainly present in La Collada and Villabona. Saddle dolomite is also found in the three districts.

Mineral precipitation ended with barite and a late generation of quartz (Q3). Barite is particularly abundant in the Berbes district, where it may constitute monomineralic veins. Barite crystals are white, tabular or prismatic in shape, and frequently form rosettes (Fig. 3D) or platy aggregates. A later event of barite precipitation has only been recognized in Villabona, where platy crystals have a characteristic pale blue colour. Late quartz (Q3) is characterized by its idiomorphic shape (Herkimer, diamond-type) and the presence of large hydrocarbon-bearing inclusions (Arcos & Tornos 1997). This late quartz generation has only been found in the Berbes district.

It is interesting to note the widespread presence of solid organic matter (bitumen) in the deposits. Bitumen is found associated with sulphides, calcite and barite. The relationship between this organic matter and the trapped hydrocarbons in late idiomorphic quartz crystals of the Berbes district remains unclear.

The distribution of gangue minerals, especially barite and sulphides, is irregular at both the deposit and district scales. In the Moscona mine, sulphides (pyrite and marcasite) and barite are particularly abundant in the northern area of the mineralization, suggesting the presence of local zonation. Sulphides are also present in La Collada and

Berbes, although in much smaller amounts. Barite is scarce in La Collada and at a regional scale it seems to be more abundant towards the east (Berbes district).

ANALYTICAL PROCEDURES

Microthermometric studies of fluid
sions from 18 samples) were carried out on doubly polished wafers (≈300 μm in thickness) with a Linkam THMSG 600 heating–freezing stage. The stage was calibrated based on the melting point of solid standards at $T > 25$•C, and natural and synthetic inclusions at $T < 0$•C. The rate of heating was monitored in order to obtain measurement precision of ±0.2•C during freezing and ±1•C when heating over the 25–400•C temperature range. The salinity of H_2O–NaCl inclusions, reported as equivalent weight% NaCl (eq. wt% NaCl), was calculated from microthermometric data (ice melting, $T_{m,ice}$) using the equations from Bodnar (1993). The salinity and composition of H_2O–NaCl–$CaCl_2$ inclusions were established from ice and hydrohalite (hydrohalite melting, $T_{m,hydrate}$) using a Microsoft Excel Add-in developed by Naden (1996). Some fluorite samples were also examined under a fluorescence microscope in order to identify any hydrocarbon-bearing inclusions.

Bulk crush-leach analyses were performed on fluorite, calcite, quartz and barite at the School of Earth Sciences, University of Leeds. The procedure has been described in detail by Banks *et al.* (2000). The samples were crushed to 1–2 mm in size and cleaned by boiling in 18.2 MΩ water. Dry samples from 0.5 to 1 g were crushed to a fine powder in an agate pestle and mortar, transferred to a sample container and the dried salts redissolved in 18.2 MΩ water. Anions (Cl^- and Br^-) were determined with a Dionex DX-500 ion chromatograph and cations (Na^+ and K^+) were determined on the same solution removed leached with an acidified $LaCl_3$ solution by flame
troscopy. The analytical precision of these analyses was better than 10% (2σ).

Laser ablation ICP-MS analyses of individual fluid
sions were carried out at the School of Earth and Environment, University of Leeds. Fluid inclusions in fluorite pieces, carefully selected after microthermometric study, were ablated with a GeoLas Q Plus Excimer Laser (ArF, 193-nm Microlas, Göttingen, Germany), using a repetition rate of 5 Hz and laser fluence
rial was transported from a cylindrical chamber with a height of 5 mm and internal diameter of 57 mm, in 0.68 l min^{-1} He via Teflon
with a volume of 9.5 cm^3, where the analytes were premixed with 0.94–0.98 l min^{-1} Ar before introduction into the plasma. Ablated samples were analysed with an Agilent 7500c quadrupole ICP-MS, equipped with an octopole reaction cell. The cell was pressurized with 2.5 ml min^{-1} H_2 which virtually eliminated $^{40}Ar^+$ and $^{40}Ar^{16}O^+$ interferences on $^{56}Fe^+$ and greatly reduced the high Ar-based backgrounds on ^{39}K. The measured isotopes were ^{23}Na, ^{24}Mg, ^{39}K, ^{55}Mn, ^{56}Fe, ^{63}Cu, ^{66}Zn, ^{137}Ba and ^{208}Pb and Na was used as the internal reference element in all cases. Data from ^{63}Cu was subsequently discarded due to interferences, probably from $^{44}Ca^{19}F$. Fluid inclusion analyses were calibrated using combinations of NIST SRM 610 and 612 silicate glass standards and a standard solution in a glass capillary. Absolute element concentrations were determined by multiplying element weight ratios to Na by the Na concentrations derived from microthermometric data and then corrected for the contribution of other major elements in the fluid
mass balance approach: $[NaCl]_{equiv} \approx [NaCl] + \sum_i [X_iCl_{ni}]$. Full details of the analytical procedure, including the ablation of standards, and data processing, are given in Allan *et al.* (2005). To ensure accurate results, ablations with Na signals below 10σ of the background were rejected. Detection limits of other elements were calculated as 3σ of the background (Longerich *et al.* 1996).

MICROTHERMOMETRY OF FLUID INCLUSIONS

Microthermometric studies were carried out on fluid
sions in fluorite,
three districts. Most fluid
nantly liquid (L) with a minor vapour (V) phase (L + V).

In fluorite,
and L + V type, with the vapour phase comprising 10% to 20% of inclusions volume. Inclusions distributed along growth planes, parallel to crystal faces (Fig. 3E) and isolated cube-shaped inclusions were considered primary (Fig. 3F). Secondary inclusions display irregular shapes and are scattered along healed fractures. They are smaller in size (5–100 μm) with a vapour proportion of 5% to 15%. In the Berbes district some inclusions containing trapped solids of brownish bitumen-like colour were also observed in fluorite.

Fluid inclusion data were also obtained from quartz (Q2) samples from Berbes and La Collada. The same quartz generation in the Moscona mine does not contain fluid
small size (less than 5 μm). Primary inclusions have regular to negative crystal shapes, are biphase (L + V) with a vapour proportion of 5–15% and are grouped along growth bands. Trails of irregularly shaped secondary inclusions (5–100 μm in size) are also abundant.

Isolated L + V inclusions (30–150 μm in size) and trails of smaller secondary inclusions (<5–50 μm) occur in calcite, and commonly show evidence for stretching and necking-down. Small, monophase L inclusions (<5–50 μm in size) are the predominant type in barite. L + V inclusions with a vapour proportion of 5–15% occurring in trails

or isolated are scarce in barite and have only been studied in samples from the Berbes and Villabona districts. Organic matter (bitumen) is occasionally present in fluid
in barite from the Berbes district. Although García Iglesias (1978) and García Iglesias and Touray (1977) described widespread secondary fluid
carbons in the Berbes district, we unfortunately found only a few of this type of inclusions, and they were too small (<5 μm) to yield usable data for this study.

On the basis of textural relationships and microthermometry, three types of fluid
type A, those containing aqueous fluid
H_2O–NaCl and type B, those containing aqueous fluid dominated by H_2O–NaCl–$CaCl_2$ that, based on salinity and $CaCl_2$ content can be subdivided into two groups, B1 and B2. All three types (A, B1 and B2) have been recognized in the Berbes, La Collada and Villabona districts, and are present in fluorite,
mary fluid
types have been observed parallel to crystal faces a long growth planes. Microthermometric results and the abbreviations used in the text are shown in Table 1 and Fig. 4. No pressure correction has been applied to the homogenization temperatures as the depth of burial at the time of ore formation (between 157 and 213 Myr) was less than 800 m (the maximum depth of the Mesozoic cover; García Iglesias & Loredo 1994), which would correspond to a hydrostatic pressure of ≈12–13 MPa.

Type A fluid inclusions

They are present as primary and secondary inclusions in fluorite,
quartz (Q2) and calcite from La Collada; and in fluorite and barite from Villabona. Their first melting temperature (T_e) is about −21°C, which corresponds to eutectic melting temperatures in the H_2O–NaCl system, suggesting that other salt species are not present in significant concentrations. The temperature of final ice melting ($T_{m,ice}$) in primary fluid
sponding to salinities between 0 and 8.2 equivalent weight per cent NaCl (eq. wt% NaCl). Homogenization occurs to the liquid phase at temperatures (T_h) between 80 and 170°C. Secondary fluid
homogenization temperatures, from 80 to 250°C. Final ice melting temperature data range from 0 to −2°C.

Type B fluid inclusions

Type B primary fluid
calcite and barite from Berbes, in fluorite
from La Collada, and in fluorite
Villabona. The first melting temperatures (T_e), between −65 and −45°C, and the brown to yellowish colour of the

Table 1 Microthermometric data from primary fluid inclusions recognized in fluorite, calcite (1), barite and quartz (Q2) from Berbes, La Collada and Villabona districts.

Components/fluid type	District	Area	Hosted mineral	$T_{m,ice}$ (°C)	$T_{m\text{-}hydrate}$ (°C)	T_h (°C)	Salinity	N
H_2O–NaCl								
Type A	Berbes	Paredona, San Lino	Fluorite, quartz (Q2), calcite 1	−4.8/0 (mode: −4.4)	–	85/170 (mode: 140)	0/7.5 eq. wt% NaCl (mode: 7)	55
	La Collada	La Viesca	Fluorite, quartz, calcite 1	−5.3/0 (mode: −1.4)	–	90/170 (mode: 120)	0/8.2 eq. wt% NaCl (mode: 2.3)	166
	Villabona	Moscona mine	Fluorite, barite	−4.9/−0.5 (mode: −4.3)	–	80/125 (mode: 90)	0.8/7.7 eq. wt% NaCl (mode: 6.8)	27
H_2O–NaCl–$CaCl_2$								
Type B1	Berbes	Paredona, San Lino	Fluorite, calcite1, barite	−9.3/−5.9 (mode: −6.3)	−22.2/−21.4 (mode: −22)	120/160 (mode: 140)	9/12.5 wt% NaCl 0.4/0.5 wt% $CaCl_2$	83
	La Collada	La Viesca	Fluorite, quartz (Q2)	−14.3/−5.5 (mode: −11.7)	−22.4/−21.4 (mode: −21.7)	110/150 (mode: 135)	12/16 wt% NaCl 0.4/2.4 wt% $CaCl_2$	84
	Villabona	Moscona mine	Calcite 1	−6.1/−5.8 (mode: −6.1)	−22.4/−21.6 (mode: −22)	135/150 (mode: 135)	7.9/8.7 wt% NaCl 0.5/1.1 wt% $CaCl_2$	6
Type B2	Berbes	Emilio mine	Fluorite, quartz (Q2)	−24.3/−23 (mode: −24)	−28/−26 (mode: −26)	115/150 (mode: 130)	9.3/12.5 wt% NaCl 11.2/14.3 wt% $CaCl_2$	25
	La Collada	La Viesca	Quartz (Q2)	−23/−17 (mode: −22)	−29/−28 (mode: −28)	95/115 (mode: 95)	7.5/9.1 wt% NaCl 11.8/14 wt% $CaCl_2$	14
	Villabona	Moscona mine	Fluorite	−22.4/−18 (mode: −20)	−27.8/−27 (mode: −27.5)	75/100 (mode: 90)	8.2/10.3 wt% NaCl 11/13.5 wt% $CaCl_2$	15

$T_{m,ice}$, last ice melting; $T_{m\text{-}hydrate}$, last hydrohalite melting; T_h, homogenization to liquid; N, number of measurements.

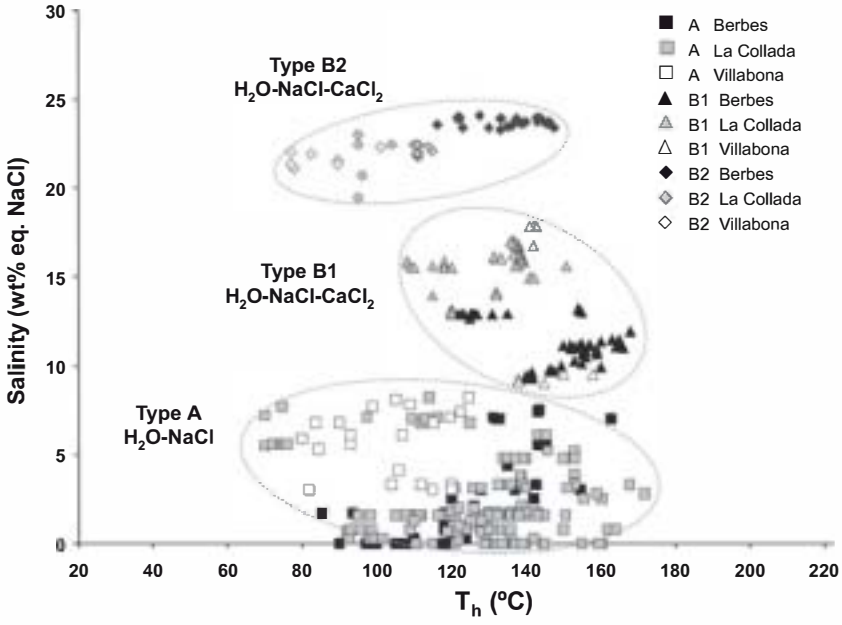

Fig. 4. Homogenization temperature versus salinity plot for H_2O–NaCl (type A primary fluid inclusions) and H_2O–NaCl–$CaCl_2$ fluids (type B primary fluid inclusions) in fluorite, quartz, calcite and barite.

liquid phase when frozen to around −100°C, are characteristic of the H_2O–NaCl–$CaCl_2$ system (Reynolds & Goldstein 1994). Based on distinct groupings in $T_{m,ice}$ and $T_{m\text{-}hydrate}$, two different types of H_2O–NaCl–$CaCl_2$ inclusions were distinguished, named B1 and B2.

B1 inclusions. These inclusions were found in fluorite, calcite and barite from Berbes, in fluorite and quartz from La Collada and in calcite from Villabona. The $T_{m,ice}$ in the three districts varied between −14.3 and −5.5°C. $T_{m,hydrate}$ occurs prior to $T_{m,ice}$ at temperatures from −22.4 to −21.4°C. Modelling these data in the NaCl–$CaCl_2$–H_2O system yields estimated bulk salinities of 8.4–18.4 wt% NaCl + $CaCl_2$, with 7.9–16 wt% NaCl and 0.4–2.4 wt% $CaCl_2$. Salinities calculated from the $T_{m,ice}$ and $T_{m,hydrate}$ in the Berbes and Villabona districts (less than 12.5 wt% NaCl and 1.1 wt% $CaCl_2$) are lower than those of La Collada (16 wt% NaCl and 2.4 wt% $CaCl_2$). B1 inclusions have homogenization temperatures to liquid between 110 and 160°C with a mode of 135°C.

B2 inclusions. These occur in fluorite and quartz from Berbes (Emilio mine); fluorite in Villabona (Moscona mine), and in quartz (Q2) from La Collada. Similar final melting temperatures have been measured in the three districts: $T_{m,hydrate}$ (−29 to −26°C) occurs before the final melting of ice ($T_{m,ice}$: −24.3 to −17°C). Calculated bulk salinity ranges from 23 to 26 wt% NaCl + $CaCl_2$ composed of 7.5–12.5 wt% NaCl and 11.0–14.3 wt% $CaCl_2$. T_h values vary between 75 and 150°C, with the lowest values in Villabona (75–100°C) and the highest values in Berbes (115–150°C).

The major solute composition of B1 and B2 fluid inclusions from the three districts, calculated from $T_{m\text{-}hydrate}$ and $T_{m,ice}$ are shown on the phase diagram for the H_2O–NaCl–$CaCl_2$ system (Fig. 5) based on Oakes *et al.* (1990). As the final melting of hydrohalite occurs before the final melting of ice, most of inclusions plot within the stability field of ice + liquid and the two populations of fluid inclusions can be distinguished. The B1 inclusions form a trend sub-parallel to the H_2O–NaCl boundary indicative of low and fairly constant $CaCl_2$ (<2 wt%) and variable NaCl contents (8–16 wt%), excluding a small group of results from La Collada. B2 inclusions plot near the centre of the diagram and are characterized by higher $CaCl_2$ and NaCl contents.

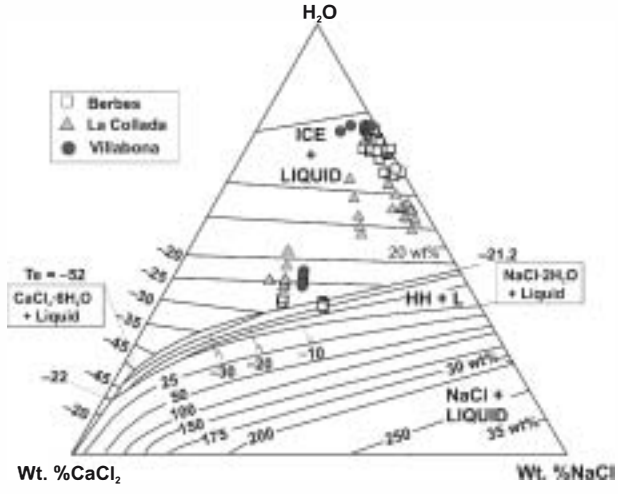

Fig. 5. H_2O–NaCl–$CaCl_2$ ratios of type B primary fluid inclusions in fluorite, quartz, calcite and barite, plotted on the diagram of Oakes *et al.* (1990).

Crush-Leach

Thirty-six samples (fluorite,
analysed for their Cl, Br, Na and K content. The halogen content (Cl and Br) and halogen ratios (Cl/Br and Na/Br) of fluid
of different fluid
the origin of their salinity (Banks *et al.* 2000). Crush-leach is a bulk analysis technique, and it does not allow discrimination between different populations of fluid
Crush-leach samples have been carefully selected in order to get a majority (>90%) of fluid
Type A fluid
(Table 2). Separation between B1 and B2 fluid
populations was not possible. Results are shown in Table 2.

Most inclusions have Cl/Br ratios lower than that of sea water (*ca.* 655) and lie on or close to the region to the sea water evaporation trend indicative of halite precipitation (Figs 6 and 7). In a Cl/Br versus Na/Br (molar) diagram, most of the data plot on or close to a line resulting from mixing, in variable proportions, of fluids with contrasting Cl/Br ratios (Fig. 6). As the most abundant type of fluid
responds to the low-salinity H_2O–NaCl fluids
these halogen ratios suggest that the predominant fluid was sea water derived. H_2O–NaCl–$CaCl_2$ fluid
(type B) have higher Cl/Br ratios, from *ca.* 1100 to 13 000, which can result from halite dissolution. Interestingly, most of the data from this group plot on the left-hand side of the halite dissolution line, suggesting a loss of Na from the fluid
fluid–rock interaction
(Davisson & Criss 1996) or a Mg–Ca exchange during dolomitization processes, thus resulting in a more Ca-rich brine.

Table 2 Leachate analysis (molar ratio) of fluid inclusions in fluorite, calcite, barite and quartz from Berbes, La Collada and Villabona districts.

District	Sample	Hosted mineral	Predominant fluid type	Cl/Br	Na/Br	Na/Cl	Na/K
La Collada	CO-04-03	Fluorite	A	872	642	0.75	13
	CO-04-16	Fluorite	A	824	601	0.74	14
	CO-04-10	Fluorite	A	263	265	1.02	15
	CO-04-07	Calcite	A	515	323	0.63	16
Berbes	BE-03-39	Fluorite	A	217	158	0.74	15
	BE-05-07b	Fluorite	A	635	481	0.77	30
	BE-05-08	Fluorite	A	298	196	0.67	25
	BE-05-14	Fluorite	A	664	519	0.79	23
	BE-05-EM	Fluorite	A	287	167	0.59	22
	BE-05-22	Fluorite	A	247	138	0.56	20
	BE-03-46	Calcite	A	229	93	0.41	15
	BE-03-49	Calcite	A	226	97	0.44	13
	BE-05-07	Calcite	A	579	495	0.87	24
	BE-05-11	Calcite	A	517	329	0.65	19
	BE-03-21	Quartz	A	616	610	1	16
	BE-03-21b	Quartz	A	630	588	0.95	15
Villabona	VI-04-02	Fluorite	A	405	291	0.73	26
	VI-04-07	Fluorite	A	323	201	0.63	21
	VI-04-10	Fluorite	A	98	70	0.73	22
	VI-04-14	Fluorite	A	701	608	0.88	38
	VI-05-FL	Fluorite	A	315	213	0.69	16
	VI-05-MFL	Fluorite	A	580	394	0.69	24
	VI-04-02	Calcite	A	601	438	0.74	32
La Collada	CO-04-03	Fluorite	B	1028	777	0.77	13
	CO-04-06	Fluorite	B	1076	791	0.74	11
	CO-04-16	Fluorite	B	3410	2582	0.77	14
	CO-04-13	Calcite	B	1151	804	0.71	13
	CO-04-17	Calcite	B	3267	2317	0.72	10
	CO-04-07	Quartz	B	1088	787	0.73	13
Berbes	BE-03-03	Fluorite	B	6977	5230	0.76	33
	BE-05-07a	Fluorite	B	1175	888	0.77	36
	BE-05-25	Fluorite	B	2130	1660	0.79	19
	BE-05-12	Barite	B	1385	1167	0.85	28
	BE-03-32	Quartz	B	12 815	10 844	0.86	14
Villabona	VI-04-15	Fluorite	B	8311	6459	0.79	30
	VI-04-14	Calcite	B	3480	2715	0.79	36
Sea water				658	564	0.86	46

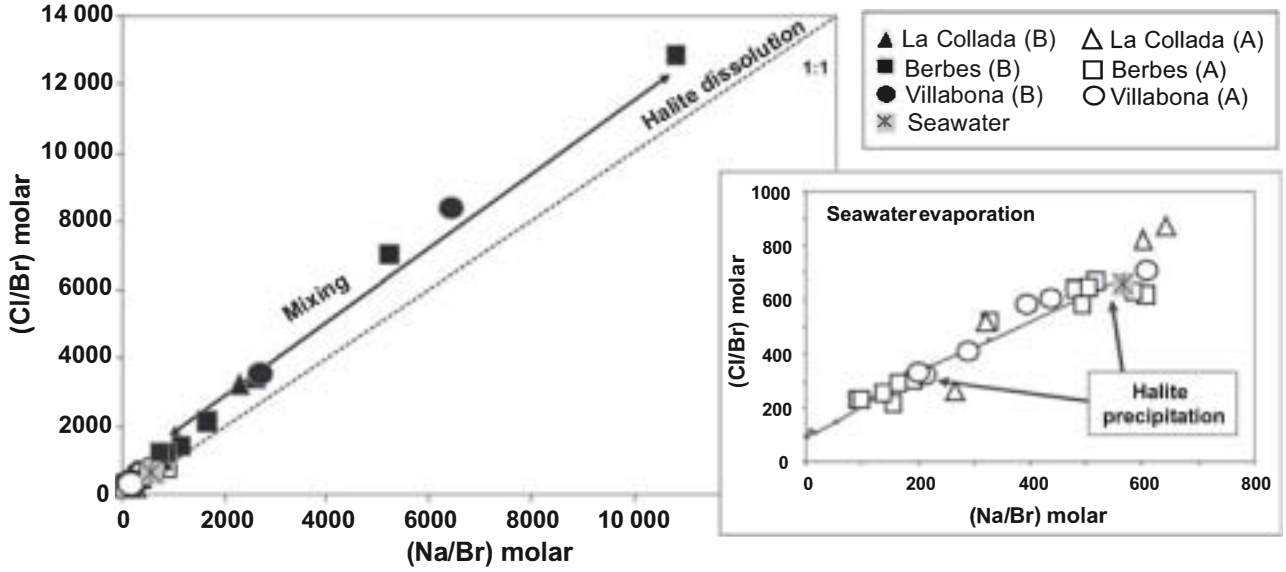

Fig. 6. Na/Br and Cl/Br molar ratios of inclusion fluids relative to evaporation of sea water and dissolution of halite. The inclusion fluids fall into two groups either from the residual brine remaining after halite precipitation from sea water or from dissolution of halite.

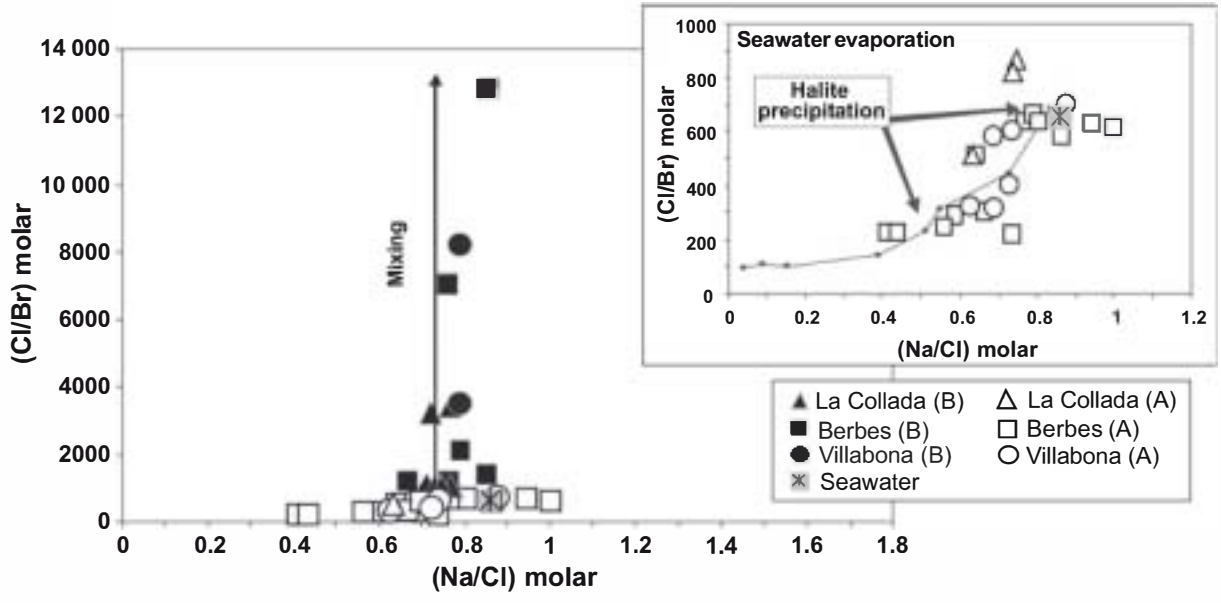

Fig. 7. Na/Cl and Cl/Br molar ratios of inclusion fluids. The vertical mixing line at a constant Na/Cl ratio of *ca.* 0.75 reveals the extent of Na loss.

In a Cl/Br versus Na/Cl diagram, most of fluid A data plot along the sea water evaporation trend (Fig. 7), indicating an evolved Br-rich fluid. However, type B fluid plots along a constant Na/Cl ratio (0.75) consistent with mixing of the Br-rich fluids (type A) with halite dissolution brine. Water–rock interaction may be recognized in a Cl/Br versus Na/K diagram (Fig. 8). Most of the Br-rich fluid inclusions (type A) plot on or close to the sea water evaporation trend, and although they exhibit different Na/K ratios, their values are consistent with the degree of evaporation as defined by Cl/Br ratios. A few samples plot further to the left, reflecting a certain degree of alteration. The fluid inclusions with variable amounts of halite dissolution fluid show a decrease in Na/K ratios with increasing Cl/Br ratios, although this correlation is the opposite of what would be expected for halite dissolution. Nevertheless, this would be explained if we consider that there has been an extensive interaction between rock and the halite dissolution fluid, the latter loosing significant amounts of Na in the process.

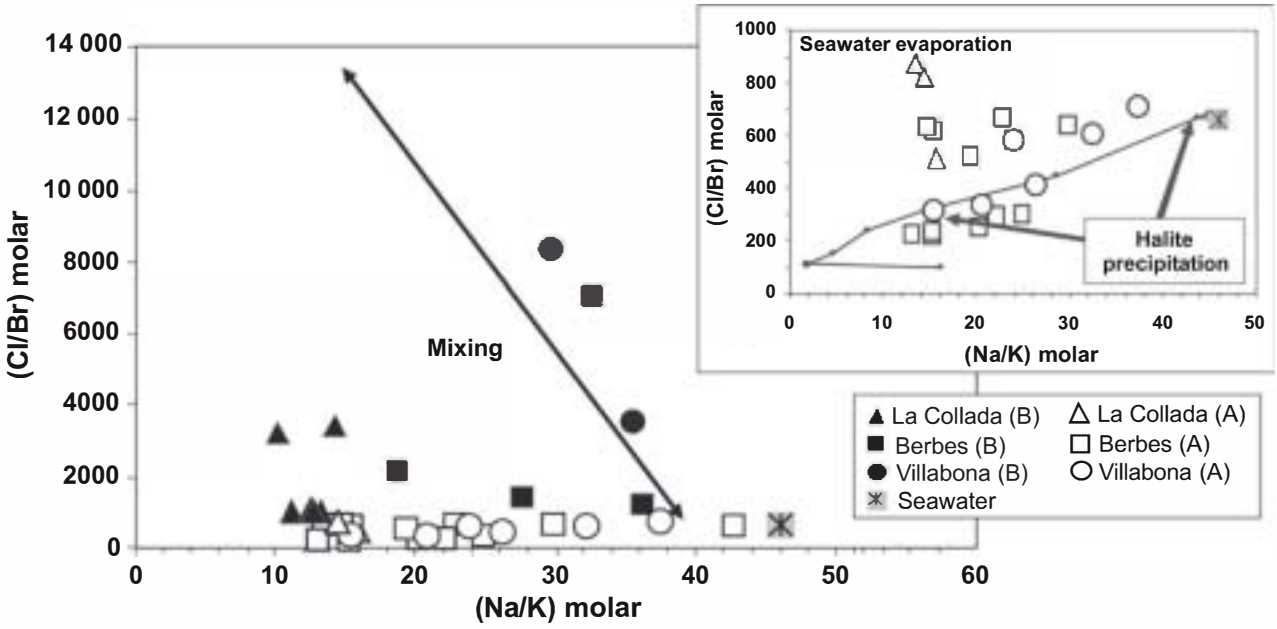

Fig. 8. Na/K and Cl/Br ratios of the inclusion fluids. The difference from the expected Na/K ratios of evaporating sea water is variable.

LA-ICP-MS analysis

LA-ICP-MS multi-element (Li, Na, Mg, K, Ca, Mn, Fe, Ba, Zn and Pb) quantitative analysis was carried out on 380 fluid inclusions in fluorite, contained in eight representative samples from the three districts, previously studied by microthermometry. The inclusions analysed ranged from 50 to 200 μm in size. Absolute concentrations and weight ratios of cations were calculated using Na as internal standard and are shown in Table 3; the Na concentration was estimated from microthermometric data.

Both type A (H_2O–NaCl) and B1 (H_2O–NaCl–$CaCl_2$) fluid inclusions were analysed in fluorite from La Paredona and San Lino mines (Berbes district) and La Viesca mine (La Collada district). B2 fluid inclusions (H_2O–NaCl–$CaCl_2$) were analysed satisfactorily only in fluorite from Emilio mine (Berbes district). In fluorite from Moscona mine (Villabona district) only type A inclusions were analysed, as type B1 and type B2 inclusions were scarce and small (<10 μm). Moreover, element concentrations in type B inclusions turned out to be inversely proportional to the Na counts. This type of correlation is probably related to an analytical artefact due to the small size of the inclusions and therefore these results were rejected.

In order to elucidate any relationship between the analysed elements, the molar ratios were plotted against each other (Fig. 9). In a Mg/Na versus K/Na plot (Fig.9A) type A fluid inclusions are more enriched in Mg than K, while type B1and type B2 fluid inclusions are more enriched in K. The K/Na ratio can be compared roughly with that obtained by crush-leach. Positive correlation trends are observed in plots like Pb/Na versus Ba/Na (Fig. 9B), Pb/Na versus Zn/Na (Fig.9C) and Fe/Na versus Zn/Na (Fig.9D). The molar abundance of the analysed metals in most fluid inclusions is Fe > Zn > Pb.

The dominant cation in the different fluid types is Na, with lesser amounts of Ca, K and Mg (Table 3). The K concentrations ranged between 2200 and 2600 p.p.m. in type A fluid inclusions and 4400–6900 p.p.m. in type B1 and type B2 ones (Fig. 10). There appears to be an increase in the K content in type B with respect to type A fluid inclusions in both the Berbes and La Collada districts. The measured Mg concentrations are between 1400 and 1850 p.p.m. in all three districts. Type B1 and type B2 fluid inclusions are also more Mg–Fe-enriched than type A ones. Mn concentration was below the detection limit in some type B1 and type B2 inclusions, but type A fluid inclusions contained between 30 and 70 p.p.m. (Table 3).

Fluids trapped in fluorite are characterized by slightly higher metal concentrations (Zn, Pb and Ba) than those observed in modern sedimentary brines, which may contain up to approximately 100 p.p.m. Pb, 250 p.p.m. Zn and 150 p.p.m. Ba (e.g. Land 1995; Hanor 1996). Type A fluid inclusions typically contain lower concentration of Fe, Zn, Pb and Ba (170–380, 70–230, 25–150, 100–310 p.p.m. respectively) than type B1 and type B2 fluid inclusions (160–500, 85–160, 320–480 p.p.m. respectively; Table 3; Fig. 10). Ba and Zn contents in type B1 fluid inclusions show intermediate values between type A and type B2 fluids. Ba, Zn and Pb contents of the inclusions with type A fluid (Fig. 10) also appear to decrease from E to W, that is from Berbes, to La Collada and to

Table 3 Summary of individual fluid inclusions analyses by LA-ICP-MS in fluorite from Berbes, La Collada and Villabona districts.

	Fluid A				Fluid B1				Fluid B2
District	Berbes		La Collada	Villabona	Berbes		La Collada		Berbes
Sample	BE03-PAR	BE03-36	CO04-03	VI04-7/10	BE03-PAR	BE03-36	CO-04-10	CO04-06	BE05-EM
Salinity*	3.0	7.2	1.6	7.0	9.4	13	18	17.5	25.4
Element molar ratios									
Mg/Na									
Average	0.12003	0.12988	0.08805	0.05512	0.02468	0.01268	0.01792	0.01430	0.04336
SD	0.08024	0.09946	0.03432	0.01473	0.01624	0.00563	0.00762	0.00510	0.01937
K/Na									
Average	0.10277	0.09079	0.09386	0.04412	0.03171	0.07734	0.06442	0.08130	0.05182
SD	0.04976	0.05046	0.03341	0.03348	0.01452	0.02118	0.01267	0.02849	0.02032
Ba/Na									
Average	0.00189	0.00294	0.00238	0.00056	0.00267	0.00021	0.00091	0.00090	0.00061
SD	0.00124	0.00077	0.00094	0.00032	0.00122	0.00008	0.00057	0.00051	0.00024
Mn/Na									
Average	0.00042	0.00089	0.00022	0.00024	0.00043	0.00018	0.00031	0.00018	0.00024
SD	0.00023	0.00006	0.00011	0.00008	0.00024	0.00001	0.00006	0.00006	0.00013
Fe/Na									
Average	0.01259	0.00488	0.00176	0.00206	0.02020	n.d.	0.00091	0.00068	0.00886
SD	0.00777	0.00015	0.00108	0.00082	0.01043		0.00051	0.00017	0.00631
Zn/Na									
Average	0.00414	0.00164	0.00646	0.00100	0.00658	0.00045	0.00059	0.00044	0.00582
SD	0.00248	0.00065	0.00210	0.00056	0.00271	0.00012	0.00028	0.00025	0.00280
Pb/Na									
Average	0.00037	0.00031	0.00188	0.00013	0.00090	0.00013	0.00019	0.00013	0.00033
SD	0.00021	0.00014	0.00111	0.00002	0.00012	0.00001	0.00007	0.00002	0.00015
Element concentration (p.p.m.)									
Na									
Average	11 888	28 204	6146	27 789	35 245	48 987	53 705	47 239	48 983
SD	18	103	20	3	27	43	2	48	55
Mg									
Average	1850	1557	1465	1598	2047	2131	1981	2795	2413
SD	1371	1032	1293	427	1538	1820	1376	2387	1491
K									
Average	2230	2634	2248	2275	4465	6424	6982	6275	5373
SD	1476	1028	1847	1581	3983	1759	3375	2647	3130
Ca†									
Average	1964	4231	922	4168	13 710	12 541	8593	19 840	41 440
SD	3	15	3	0	10	11	0	20	47
Ba									
Average	312	303	125	109	404	439	325	385	482
SD	239	223	94	50	277	391	269	313	328
Mn									
Average	69	43	51	33	n.d.	37	46	n.d.	40
SD	19	30	35	26		24	34		24
Fe									
Average	324	234	382	171	374	n.d.	886	1111	1015
SD	91	176	267	107	265		167	934	819
Zn									
Average	237	177	208	76	161	404	334	339	493
SD	139	128	174	53	121	345	272	294	338
Pb									
Average	86	63	153	26	166	92	116	87	107
SD	51	43	101	6	85	66	70	59	59
No. of inclusions	45	13	82	44	73	34	31	25	40

n.d., not detected.

*Modal salinity of fluid inclusions in eq. wt % NaCl.

†Calculated using average Ca/Na ratios from $T_{m\text{-}hydrate}$ data for fluid B (0.38 was used for sample BE03-PAR, 0.25 for sample BE03-36, 0.84 for sample BE05-EM, 0.42 for sample CO04-06, 0.16 for sample CO04-10) and LA data in quartz (Q2) fluid inclusions for fluid A (0.15 in all samples).

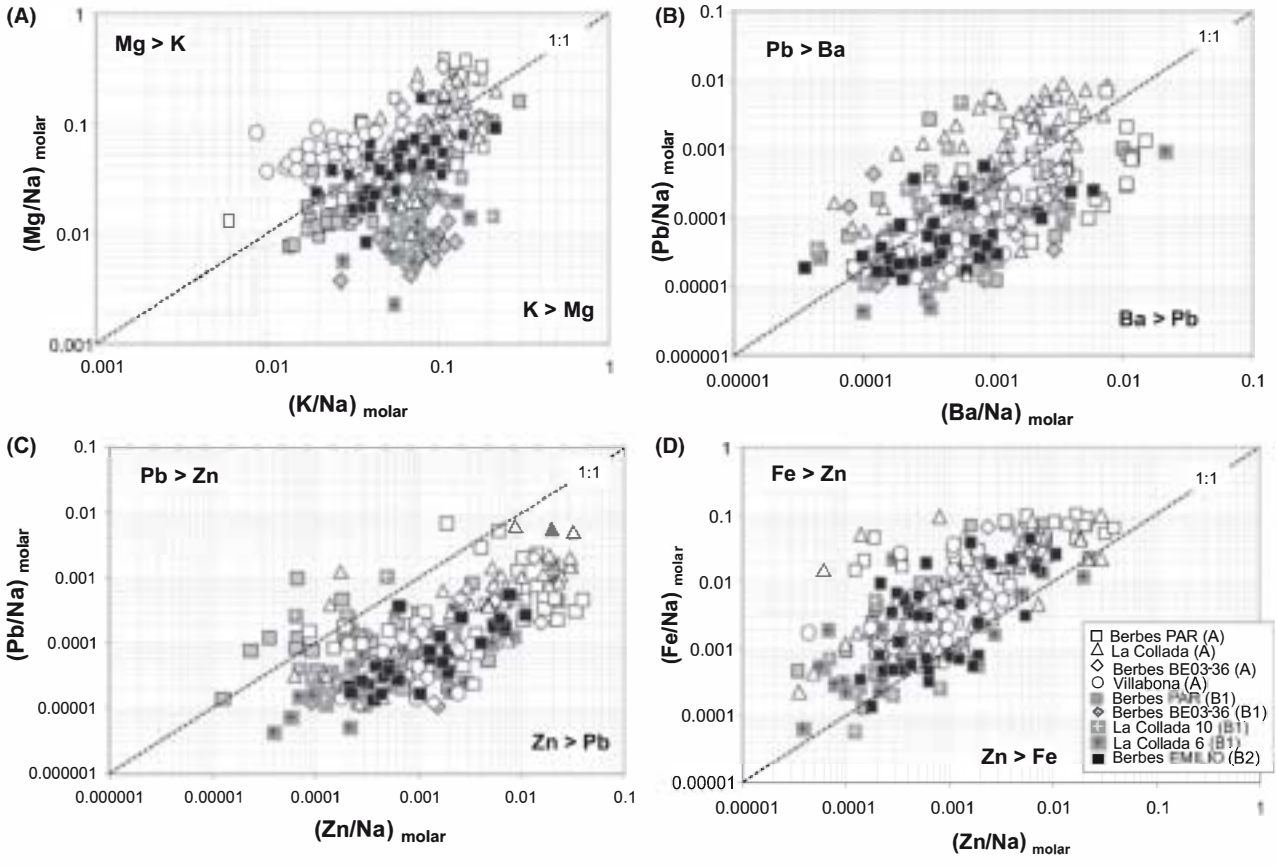

Fig. 9. Individual fluid inclusions data plots from LA-ICP-MS analysis. (A) Mg/Na versus K/Na molar ratios (B) Pb/Na versus Ba/Na molar ratios (C) Pb/Na versus Zn/Na and (D) Fe/Na versus Zn/Na in fluid inclusions from Berbes, La Collada and Villabona fluorite samples.

Villabona districts. Interestingly, barite predominates in fluorite deposits situated to the E of the area studied (Berbes and La Collada).

DISCUSSION

Source of the fluids

The contrasting salinities (0–8.2 and 8.4–26.8 eq. wt% NaCl) and halogen ratios (Cl/Br_{molar} 100–700 and 700–13 000 and Na/Br_{molar} 20–700 and 700–11 000) suggest that at least two fluids were involved and that mixing was the dominant process during fluorite precipitation over the temperature range of 80–160°C. A mixing hypothesis is also supported by Cl/Br versus Na/Cl and Cl/Br versus Na/K plots (Figs 7 and 8). One end-member was a brine originated after dissolution of evaporites as suggested by its high salinity, high $CaCl_2$ content and high Cl/Br and Na/Br ratios. The other end-member, as indicated by the low Cl/Br and Na/Br ratios, acquired its low salinity by dilution of Br-enriched evaporated sea water, suggesting the existence of a third fluid, possibly meteoric water. Therefore, fluid inclusions in fluorite are samples of the fluid mixture, at different proportions, of the end-members. Whereas salinity of type A and type B2 fluid inclusions would be close to the assumed end-members, the salinity of type B1 inclusions would correspond to a contribution of similar proportions of both end-members (see Fig. 4, T_h/salinity plot).

Most fluids trapped in type B inclusions show a loss in Na (Fig. 6) as deduced from microthermometric measurements and possible Ca enrichment. Both characteristics are compatible with the expected evolution of a brine after its interaction with plagioclase-rich rocks, which are present both in the Palaeozoic basement and in the Permo-Triassic series (i.e. trachyandesites). Taking into account that the value of Mg is lower than it should be expected in evaporating sea water, the gain of Ca could be the result of a Mg–Ca exchange during dolomitization processes.

Fluid composition and basinal differences

The average concentrations in the three districts indicate that the dominant cation in the fluid mixtures is Na, with lesser amounts of Ca, K and Mg. Compared with the evaporated sea water (fluid A), the brine (fluid B) is enriched in